Proceedings of the 17th World Congress
The International Federation of Automatic Control
Seoul, Korea, July 6-11, 2008

Design and control of an electromagnetically actuated punch

Matthias Dagen * **Bodo Heimann** * **Mohsen Javadi** **
Bernd-Arno Behrens **

* *Institute of Robotics, Leibniz Universität Hannover, Hannover, Germany (e-mail: {dagen, heimann}@ifr.uni-hannover.de)*
** *Institute of Metal Forming and Metal Forming Machine Tools, Leibniz Universität Hannover, Hannover, Germany (e-mail: {javadi, behrens}@ifum.uni-hannover.de)*

Abstract: In this paper a new electromechanically actuated punch (EAP) is presented. This punch can apply forces up to 10 kN and has a stroke up to 4 mm. Due to the high dynamics drive-concept, the ram's kinematics is changeable during the punch process and backlashes are non-existent. Therefore, the punch is especially qualified for manufacturing micro-components demanding high accuracy and high stroke rates. A control concept is introduced, which can handle constraints and windup effects. Finally, experimental results are given.

1. INTRODUCTION

Within the last years the importance of manufacturing micro-components in metal forming increased while at the same time the requirements regarding accuracy of the micro-components also increased. Due to the elements' high output levels, they are usually produced on mechanical high-speed presses. Such presses are able to reach stroking speeds up to 4000 strokes per minute and nominal forces up to 2000 kN. These presses transform the revolute motion of the electric motor into the linear motion of the ram. But the use of mechanical high-speed presses causes several drawbacks. The sinus-shaped kinematics of the ram can only be adjusted by complex lever kinematics and non-circular gears (Hindersmann and Doege [1997]). Thus, a change of the kinematics is impossible during operation. Furthermore the backlash of the gear elements leads to a decreasing accuracy of the punchings. Additionally, these presses provide a much higher power than the production of micro-components requires. In contrast, hydraulic presses are able to change the ram's kinematics, but their dynamics does not allow an economic production of micro-components.

The given preferences of conventional presses illustrate the necessity of a new economic, accurate and innovative drive-concept. To fullfill this need, Schuler et al. developed a press called *Stanzrapid* (Schepp [2001], Schneider [2004]). It uses two prismatic actuators in order to achieve the required forces. This concept allows an online adjustment of the ram's kinematics. Currently, punch-forces up to 40 kN and stroking speeds up to 1200 strokes per minute are achievable. But, the prismatic actuators suffer from a low degree of efficiency resulting in a high waste heat. Therefore, an additional cooling unit is required. Furthermore, the achievable strokes per minute are significantly lower in comparison to existing punches.

Former inventions of Meyerle [1998], Doherty [1973] and Boye [1981] use electrodynamic effects to move the ram but without any control. The achievable ram velocity of such presses is high, but the non-adjustable ram kinematics, the high tool wear level and the high noise emissions are negative effects of this approach.

As a result of the given facts we present an innovative approach for presses using the reluctance forces of electromagnets to actuate the ram. An excellent example of such drive-concept is given in Wang [1996] and Oberbeck [2003] who use this concept for vibration excitation. The advantage of our approach is the lack of any gearboxes in combination with very small friction. This results in higher accuracy and dynamics which allows high stroking rates. Furthermore, the proposed actuation concept leads to a great dynamics behavior and a very compact architecture. In contrast to the *Stanzrapid*, no additional cooling unit is necessary. Additionally, due to innovative control concepts it is possible to improve the accuracy while punching and change the ram's kinematics if necessary.

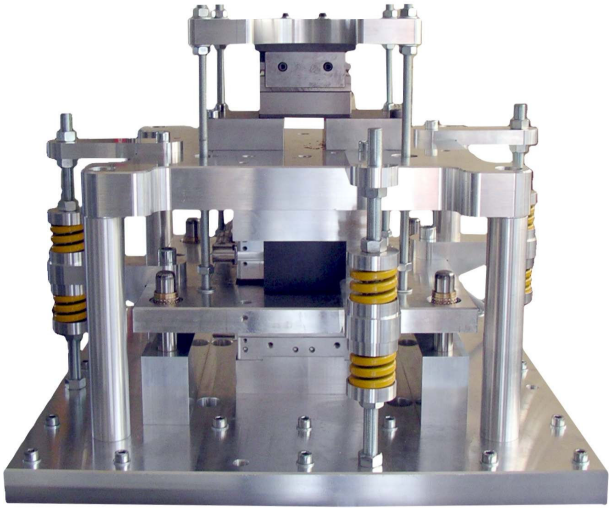

Fig. 1. Prototype of the EAP

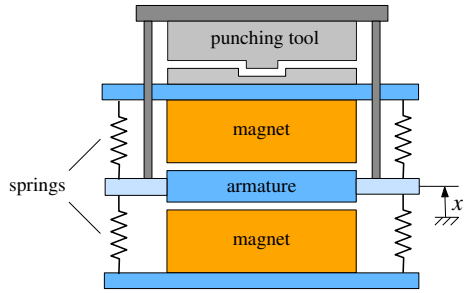

Fig. 2. 2D-scheme of the EAP

Figure 1 shows the first prototype of our electromagnetic actuated punch with forces up to 10 kN at each position and a maximum stroke of 4 mm.

This paper is organized as follows. In section 2 the design of the punch and its components are described briefly. Section 3 shows a concept to linearize the characteristic force diagram of the electromagnets. Section 4 gives an overview of the control design. Especially a method to avoid the windup effect due to the PI-state feedback control and the constraint electromagnetic force is described in detail. In section 5 practical results of the punch are presented. Section 6 completes the paper with the conclusions.

2. SYSTEM DESIGN

Figure 2 shows a 2D-scheme of the proposed punch. Two high-performance electromagnets are positioned in opposition. The armature in the middle is guided by four linear bearings. Eight heavy duty springs are placed between the armature and the frame. The benefit of the chosen arrangement is the static relation between the coil current and the air-gap which results in a more linear force relation. Furthermore, the springs allow high forces at positions where the electromagnetic force is naturally limited (see section 3).

The two E-shaped electromagnets consist of three poles with a pole face of 144 cm^2 and a coil with 100 windings. To allow high coil currents and to reduce the heating of the electromagnets we use a copper wire with a rectangular profile and a cross-section area of 4.2 mm^2.

Due to the conductivity of the magnetic core and the armature eddy currents are generated by the alternating magnetic flux. According to the Lenz's law they create a new magnetic field that oppose the effect of the applied electromagnetic field. In order to reduce these field the core and the armature consist of isolated sheets. The benefit is, that this reduces the eddy currents physically and no other measures such high-pass filters which enlarge the measurement noise have to be taken. The drawback of this

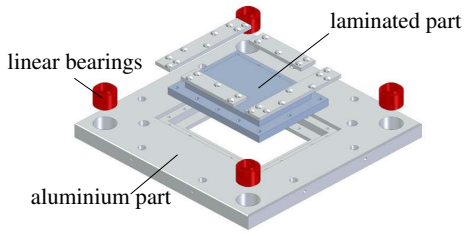

Fig. 3. 3D-model of the armature

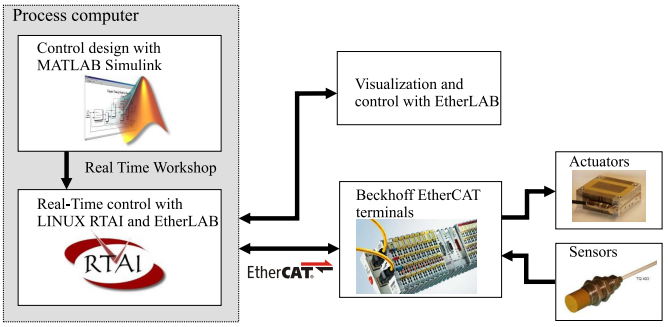

Fig. 4. Controller implementation and information flow between MATLAB Simulink, Etherlab and the Beckhoff terminals

approach is that only axis-symmetric electromagnets are possible.

In order to reduce the inertia and to enlarge the system dynamics, aluminium is used for the outer part of the armature (see fig. 3). The frame itself is also made out of aluminium to avoid secondary magnetic circles.

The armature's position is measured with a commercial eddy current sensor. It is a robust method regarding dirt and electromagnetic fields produced by the magnets. It provides a high cut-off frequency of 20 kHz. The drawback of this sensor is its non negligible non-linearity which has to be measured and taken into account (vibro-meter SA [2006]).

The punching tool is assembled at the top of the electromagnetic actuator. Its movable parts are connected to the armature via rods. This allows an absolute flexibility in choosing different kinds of tools.

For control purposes Beckhoff terminals in combination with the Linux real-time extension RTAI is used. The terminals communicate with the process computer via Beckhoff's real-time ethernet protocol EtherCAT. Additionally, Simulink Real Time Workshop® from The MathWorks in combination with the open source project EtherLab (IgH [2007]) is used to reduce coding and debugging time. The concept allows sampling rates up to 10 kHz. Up to now, we use a control loop sampling rate of 4 kHz. Figure 4 illustrates the information flow of the resulting rapid control prototyping system.

3. MODELING

The punch can be split into a mechanical and electrical subsystem. Figure 5 shows the model of the substituted mechanical system consisting of the anchor-mass m, the springs c, the velocity proportional damper b and the

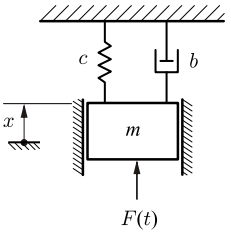

Fig. 5. Substituted mechanical system

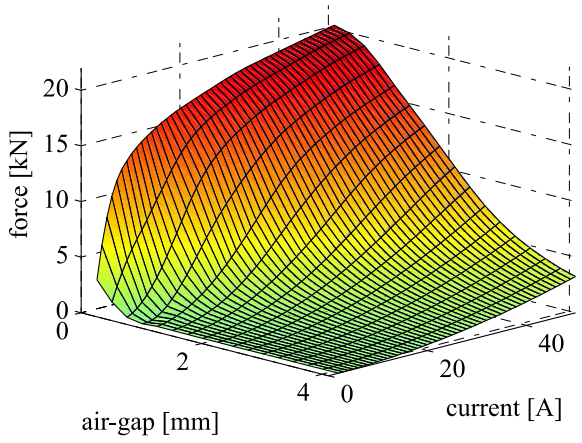

Fig. 6. Characteristic diagram of the calculated electromagnetic force

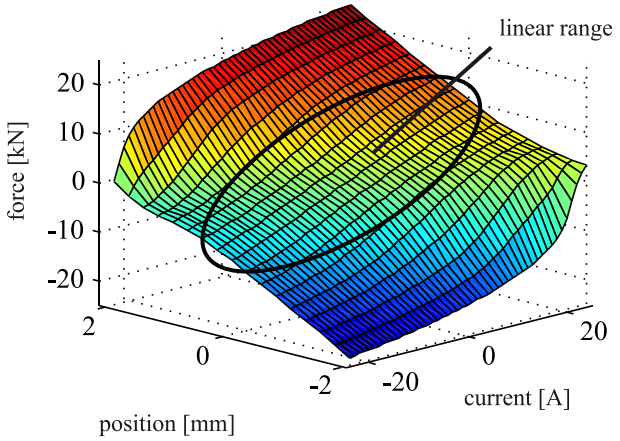

Fig. 7. Characteristic force-diagram of the actuator

electromagnetic force $F(t)$. Due to the high forces and the linear bearings the Coulomb friction is negligible. Thus, we get the following linear equation of motion;

$$m\ddot{x}(t) + b\dot{x}(t) + cx(t) = F(t). \tag{1}$$

The reluctance force $F(t)$ originates from the continuity of the magnetic flux at the boundary layer of different permeability, in this case the permeability of iron and air. In the following a short overview of the electromagnetic force calculation is given.

Using the virtual work we get the relation between the electromagnetic force F and the magnetic flux density B (Tanabe [2005])to

$$F = \frac{B^2 A}{2\mu_0}, \tag{2}$$

where A is the pole face and μ_0 the magnetic permeability in vacuum.

The analytic calculation of the real magnetic flux density with respect to the coil current and the air-gap is only possible approximately due to the non-linear behavior of the materials. If we neglect the saturation of the material we get

$$F = \frac{A\mu_0(nI)^2}{8s^2} \tag{3}$$

with the number of coils n and the actual air-gap s. Eq. (3) is eligible to construct an electromagnet approximately. For a more precisely calculation a finite element program, which considers the non-linear material's behavior and the magnetic leakage flux as well, is recommended. Because at very small air-gaps and high coil currents the magnetic field strength is high and the material is in saturation, the permeability is not constant anymore. Therefore, we use the finite element software ANSYS to calculate the non-linear characteristic force diagram shown in figure 6.

The total system consists of two inputs, the currents i_1 and i_2 of the electromagnets and two outputs, the air-gaps s_1 and s_2. In order to simplify the multi input multi output system Wang [1996] uses a differential arrangement for such a system. Thus, the air-gap of each electromagnet is given by

$$s_1 = s_0 + x, \tag{4}$$

$$s_2 = s_0 - x, \tag{5}$$

where s_0 is the air-gap of the electromagnets when the armature is located on the central position. Furthermore, a control current i and a pre-current i_0 are established. Therefore, the currents in the coils are calculated to

$$i_1 = i_0 + i, \tag{6}$$

$$i_2 = i_0 - i. \tag{7}$$

The computed force for two electromagnets in difference arrangement gives us the characteristic force-diagram of the actuator. Its advantage is, that the force is nearly linear, depending on the measured position of the armature x and the control current i in a wide range. Figure 7 demonstrates this effect.

The electrical subsystem can be modeled by an ohmic resistor R and an inductance L. Applying Kirchhoff's voltage law we get the relation between the actual current $i_\mathrm{a}(t)$ and the input voltage $u(t)$ to

$$L\frac{di_\mathrm{a}(t)}{dt} + Ri_\mathrm{a}(t) = u(t). \tag{8}$$

Additionally, a power amplifier with P-control is used to improve the dynamics behavior. In this case we get the relation between the current $i_\mathrm{a}(t)$ and the desired current $i_\mathrm{d}(t)$ to

$$\frac{di_\mathrm{a}(t)}{dt} = -\frac{R + k_\mathrm{PA}}{L} i_\mathrm{a}(t) + \frac{k_\mathrm{PA}}{L} i_\mathrm{d} \tag{9}$$

with the feedback gain k_PA.

Due to (3), the system consisting of the power amplifier and the electromagnets is highly nonlinear. To control the whole the system, it is desirable to linearize it. In our approach, we insert the inverse characteristic diagram of the electromagnets force. Therefore, we get approximately a linear correlation between the desired and the actual force shown in figure 8.

In order to design our control in the next section a state space representation given by

$$\begin{aligned} \dot{\mathbf{x}} &= \mathbf{A}\mathbf{x} + \mathbf{B}u, \\ y &= \mathbf{C}^T\mathbf{x} + Du \end{aligned} \tag{10}$$

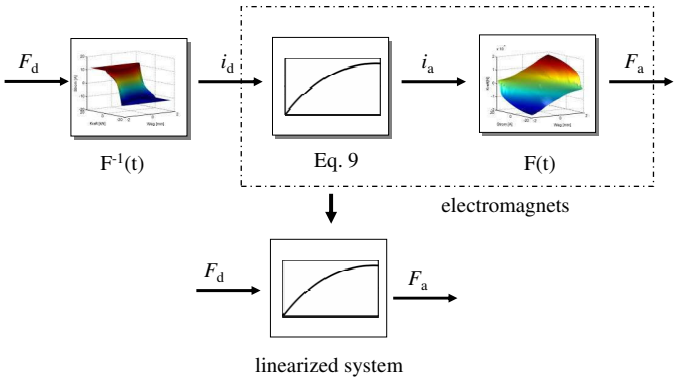

Fig. 8. Linearization of the characteristic electromagnet's force diagram

is required. Thus, using equation (1) and (9) as well as the described linearization for the electromagnets the state space representation is given as follows:

$$\dot{\mathbf{x}} = \begin{bmatrix} \dot{x} \\ \ddot{x} \\ \dot{F}_a \end{bmatrix} = \begin{bmatrix} 0 & 1 & 0 \\ -\frac{c}{m} & -\frac{b}{m} & \frac{1}{m} \\ 0 & 0 & -\frac{(k_{PA}+R)}{L} \end{bmatrix} \begin{bmatrix} x \\ \dot{x} \\ F_c \end{bmatrix} + \begin{bmatrix} 0 \\ 0 \\ \frac{k_{PA}}{L} \end{bmatrix} F_d \qquad (11)$$
$$y = [1\ 0\ 0]\,\mathbf{x}$$

4. CONTROL DESIGN

The linear state space formulation (11) allows us the use of state feedback controller. But, due to the high disturbances excited by the punching process, the general drawback of this concept, the steady-state error as a result of the missing integrator is not negligible.Therefore, a PI-state feedback control is used to stabilize our system. A second problem arises due to the interaction of the integrator and the limited force of the electromagnets. If the controller demands too high forces the actuators cannot afford, the control deviation will be too big. In this case the integral overflows (windup). Therefore, the command variable overshoots and in the worst case the system gets unstable. To avoid this behavior, anti-windup (AW) methods described by Bühler [2000] are used in this work. In the following, a brief introduction to discrete PI-state feedback control and AW-methods are given.

First of all the continuous system (11) needs to be discretized to

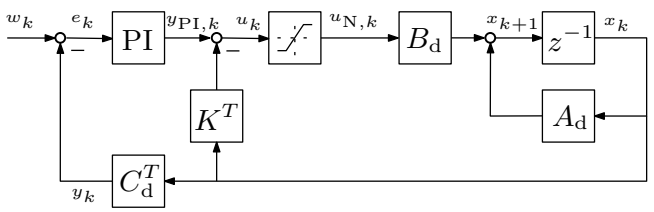

Fig. 9. Block diagram of the PI state feedback control

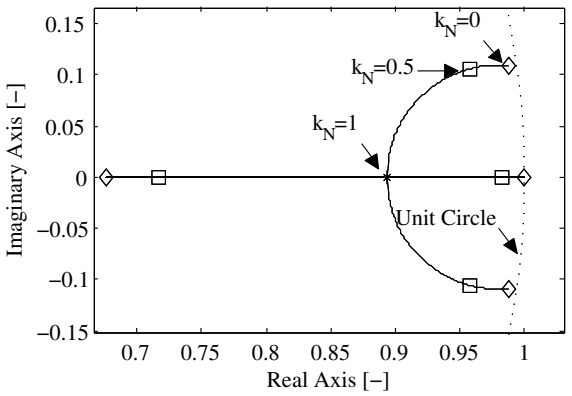

Fig. 10. Modification of the system's roots due to the constraint force

$$\begin{aligned} \mathbf{x}_{k+1} &= \mathbf{A}_d \mathbf{x}_k + \mathbf{B}_d u_k, \\ y_k &= \mathbf{C}_d^T \mathbf{x}_k. \end{aligned} \qquad (12)$$

In a state feedback control, a prefilter is used in order to set a reference point unequal zero. Using a PI state feedback control, this prefilter is replaced by a PI-block as shown in figure 9 with the state space formulation

$$\begin{aligned} x_{PI,k+1} &= x_{PI,k} + e_k, \\ y_{PI,k} &= k_I x_{PI,k} + k_P e_k, \end{aligned} \qquad (13)$$

where k_P is the proportional and k_I the integrator gain.

The saturation of the electromagnetic force can be modeled with a nonlinear gain k_N given by

$$k_N = \frac{u_{max}}{u} = \frac{f(u,y)}{u}, \qquad (14)$$

which is a function of the input u_k and the current position y_k. This means, if the electromagnets are not in their limit, the gain will be equal one, otherwise the gain will be between zero and one.

Figure 9 shows the block diagram of the closed loop system with PI-state feedback control and saturation for the input vector. Placing (13), (14) and the feedback state vector K into (12), we get the following state-space representation of the closed-loop system:

$$\begin{bmatrix} \mathbf{x}_{k+1} \\ x_{PI,k+1} \end{bmatrix} = \begin{bmatrix} \mathbf{A}_d - k_N \mathbf{B}_d (\mathbf{K}^T + k_P \mathbf{C}_d^T) & k_N \mathbf{B}_d k_I \\ -\mathbf{C}_d{}^T & 1 \end{bmatrix} \begin{bmatrix} \mathbf{x}_k \\ x_{PI,k} \end{bmatrix} + \begin{bmatrix} k_N \mathbf{B}_d k_P \\ 1 \end{bmatrix} w_k. \qquad (15)$$

To parameterize our controller, we first assume, that the limitation will never be achieved. In this case k_N is equal one and we can set the parameters k_I, k_P and the vector K. For that, we use the condition that the stationary gain of the system should be one. Thus, the proportional gain k_P becomes to

$$k_P = \frac{1}{\mathbf{C}_d{}^T (1 - \mathbf{A}_d)^{-1} \mathbf{B}_d}. \qquad (16)$$

Via pole placement we get the desired parameters K and k_I.

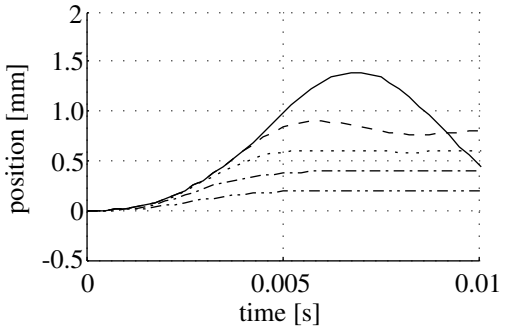

Fig. 11. Simulated step response to different input steps without anti-windup

Nevertheless, as a result of measuring only the position of the armature, the state vector $\mathbf{x}_k$ is not completely known. Hence, the non-measured states are observed by a Kalman-filter. The disturbances caused by the punch process and non-modeled dynamics are taken into account using an additional state in the observer. This leads to an increasing estimation quality, especially concerning the observed velocity.

In order to achieve a high dynamics behavior, a high control gain is essential. But this demands high input values and the saturation will often be reached. Figure 11 shows the response on several input steps. At low steps, the demanding input value is small enough and the system reacts as desired. But at higher steps, the saturation is reached and the system starts to overshot and oscillate. Thus, the nonlinear gain k_N is no longer equal one but between zero and one as mentioned before. At this time the eigenvalues of the closed loop system are not longer the provided ones but change their values due to the value of k_N. Figure 10 shows the root locus of the system with respect to k_N. At $k_\mathrm{N} = 1$ all roots are on the real axis. At $k_\mathrm{N} < 1$ two branches form and get close to the unit circle. Thus, the system is less damped. The remaining two branches stay on the real axis and have an inferior relevance for the system's characteristics.

This problem could be solved by decreasing the control gain, which would waste the overall control performance. A superior solution is to decrease the integrator only in case the saturation is reached. This results in decreased system's dynamics only during short periods of time while having full dynamics otherwise. In order to reduce the integrator, the difference between u and u_N is multiplied with the gain k_k and negatively returned. Figure 12 illustrates this. Therefore, the calculation of x_PI is given by

$$x_{\mathrm{PI},k+1} = x_{\mathrm{PI},k} + e_k - k_\mathrm{k}(u_k - u_{\mathrm{N},k}), \tag{17}$$

$$= x_{\mathrm{PI},k} + e_k - k_\mathrm{k}(1 - k_\mathrm{N})u_k. \tag{18}$$

Hence, if the saturation is reached, the integrator will be decreased and the input values also decrease. As a result, the system does not overshoot and remains stable. Figure 13 illustrates such a behavior for our system. It is obvious that the dynamics for low steps are still high and will be reduced for higher steps if necessary.

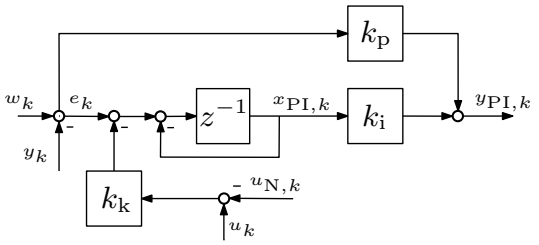

Fig. 12. PI control with anti-windup

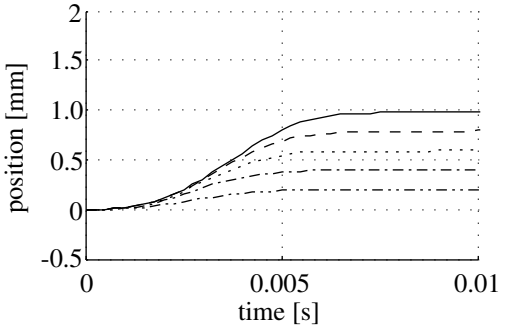

Fig. 13. Simulated step response to input steps with anti-windup

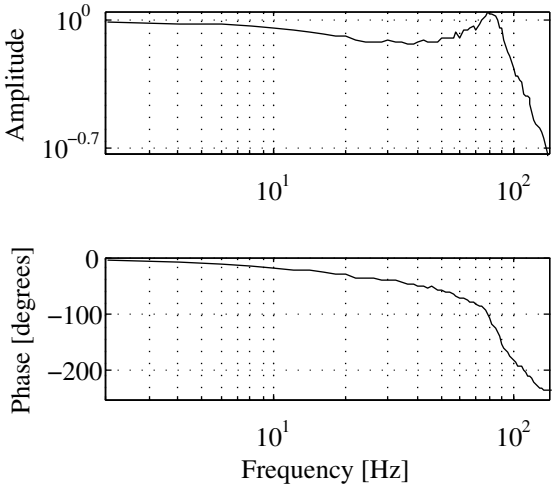

Fig. 14. Measured transfer function of the system with PI state feedback control

The choice of k_k is important to the behavior of the system. Therefore, Bühler [2000] proposes to set $k_\mathrm{k} \geq \frac{1}{k_\mathrm{i}}$. In our approach $k_\mathrm{k} = \frac{1}{k_\mathrm{i}}$ gives good results.

5. RESULTS

In the following, some results are presented. First, the transfer function was measured in the range between 1 and 110 Hz. Figure 14 shows the magnitude and phase plot of the system. In spite of the small peak at 80 Hz the system seems to have an acceptable damping characteristic.

Punching operations with a 0.4 mm thick copper sheet were performed. A picture of the punched elements, which is taken with a scanning electron micrograph (SEM) is shown in figure 15. These pieces were punched with the tool illustrated in figure 16. In the first experiments two die elements have been used for punching operations.

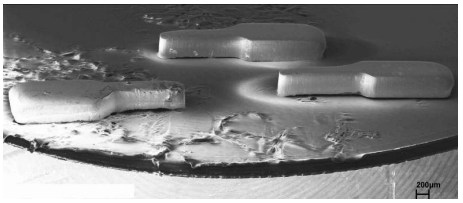

Fig. 15. SEM-picture of the punched elements

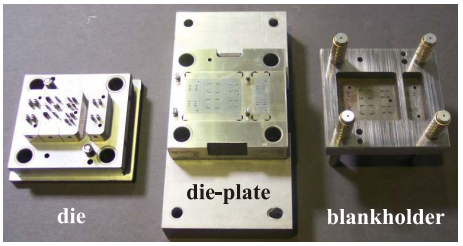

Fig. 16. Punching tool used for punch operations

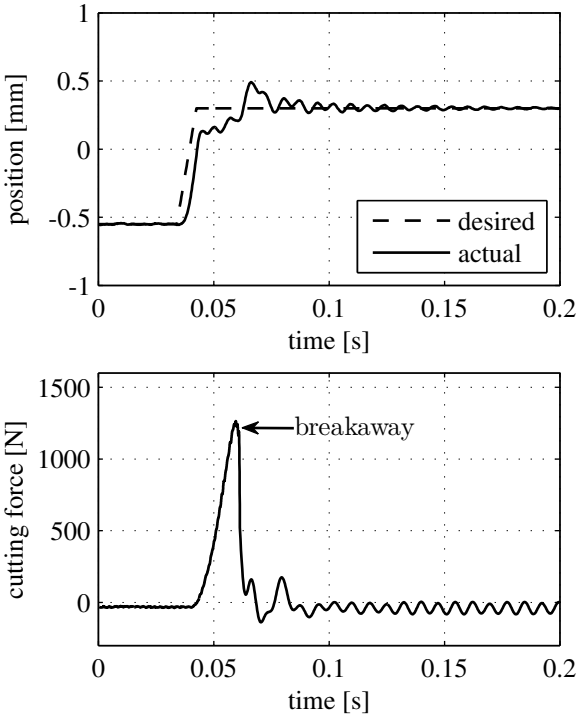

Fig. 17. Punch operation: (top) position-time plot, (middle) control deviation-time plot and (bottom) force-time plot

Therefore, approximately 1200 N are necessary to cut them out of the sheet

Figure 17 shows a position and force plot of one punch operation with a time-span of approx. 0.05 s. At the time, the ram contacts the sheet, high transient forces arise and influence the armature position. Therefore, a control deviations occurs. The following breakaway of the ram results in a high force drop, which causes a small peak. As a consequence, small vibrations are observable afterwards. Nevertheless, the control is still stable and takes the armature back to its desired position within a short time span. Up to now, the control is not capable to avoid the control deviation at the beginning. Increasing the feedback gain would improve the quality of control, but due to the existing sensor noise this it not recommend.

6. CONCLUSIONS

In this paper, an innovative drive-concept for punches was presented. After a short overview of the today's production of micro-components, the punch's design and its components were described in detail. With the proposed concept, the ram's kinematics can be adjusted on the actual cutting process. Hence, the accuracy of the punched elements can be improved. The implemented PI-state feedback control with the additional anti-windup control was illustrated. Finally, the feasibility of the electromagnetic actuated punch was demonstrated by an exemplarily punch operation.

REFERENCES

J. Boye. *Elektrodynamische Hochgeschwindigkeitspresse.* Kernforschungszentrum Karlsruhe GmbH, 1981.

H. Bühler. *Regelkreise mit Begrenzungen.* VDI Verlag Düsseldorf, 2000.

N. R. Doherty. *Electrically Actuated Punch Press.* United States Patent US-3709083, US-4022090, 1973.

M. Hindersmann and E. Doege. Optimized kinematics of mechanical presses with noncircular gears. CIRP Annals - Manufacturing Technology, v 46, pages 213–216. Universität Hannover, Institute of Metal Forming and Metal Forming Machine Tools, 1997.

IgH. *Etherlab: An Open Source Toolkit for rapid real time code generation under Linux using Simulink/RTW - and EtherCAT-Technology.* 2007. URL `www.etherlab.de`.

G. M. Meyerle. *Stanzpresse mit magnetisch isoliertem elektromagnetischen Antriebsmotor.* Europäische Patentschrift EP 0 554 258 B 1, DE 691 28 149 T 2, 1998.

Claus Oberbeck. *Entwicklung und mechatronische Optimierung eines elektromagnetischen Aktors.* PhD thesis, Institut für Angewandte Mechanik, München, 2003.

Frank Schepp. *Linearmotorgetriebene Pressen für die Stanztechnik.* PhD thesis, Institut für Produktionstechnik und Umformmaschinen, Technische Universität Darmstadt, 2001.

Roland Schneider. *Entwicklung einer Methode zur Optimierung von Fertigungsmaschinen für die Mikroumformtechnik am Beispiel von Linearmotorpressen.* PhD thesis, Institut für Produktionstechnik und Umformmaschinen, Technische Universität Darmstadt, 2004.

Jack T. Tanabe. *Iron dominated electromagnets : design, fabrication, assembly and measurements.* World Scientfic, Singapore, 2005.

vibro-meter SA. *Manual: TQ 403 Eddy Current Sensor.* vibro-meter SA, 2006.

Yongxing Wang. *Berechnung und Auslegung von Magnetstellgliedern mit Strom-Vormagnetisierung und mit Permanentmagnet-Vormagnetisierung.* PhD thesis, Institut für Mechanik, Universität Essen, 1996.